



# Predicted contextual modulation varies with distance from pinwheel centers in the orientation preference map

SUBJECT AREAS:  
MODELLING  
NEUROIMAGING  
SENSORY SYSTEMS  
IMAGING

Tsuyoshi Okamoto<sup>1</sup>, Koji Ikezoe<sup>2</sup>, Hiroshi Tamura<sup>2</sup>, Masataka Watanabe<sup>3</sup>, Kazuyuki Aihara<sup>4</sup>  
& Ichiro Fujita<sup>2</sup>

<sup>1</sup>Faculty of Medical Sciences, Kyushu University, 3-1-1 Maidashi, Higashi-ku, Fukuoka 812-8582, Japan, <sup>2</sup>Graduate School of Frontier Biosciences, Osaka University and CREST, JST, 1-3 Machikaneyama, Toyonaka-shi Osaka 560-8531, Japan, <sup>3</sup>Graduate School of Engineering, University of Tokyo, 7-3-1 Hongo, Bunkyo-Ku, Tokyo 113-8656, Japan, <sup>4</sup>Institute of Industrial Science, University of Tokyo, 4-6-1 Komaba, Meguro-Ku, Tokyo 153-8505, Japan.

Received  
9 June 2011

Accepted  
28 September 2011

Published  
12 October 2011

Correspondence and requests for materials should be addressed to T.O. (okamoto@digital.med.kyushu-u.ac.jp)

**In the primary visual cortex (V1) of some mammals, columns of neurons with the full range of orientation preferences converge at the center of a pinwheel-like arrangement, the ‘pinwheel center’ (PWC). Because a neuron receives abundant inputs from nearby neurons, the neuron’s position on the cortical map likely has a significant impact on its responses to the layout of orientations inside and outside its classical receptive field (CRF). To understand the positional specificity of responses, we constructed a computational model based on orientation preference maps in monkey V1 and hypothetical neuronal connections. The model simulations showed that neurons near PWCs displayed weaker but detectable orientation selectivity within their CRFs, and strongly reduced contextual modulation from extra-CRF stimuli, than neurons distant from PWCs. We suggest that neurons near PWCs robustly extract local orientation within their CRF embedded in visual scenes, and that contextual information is processed in regions distant from PWCs.**

Neurons in the primary visual cortex (V1) of cats and monkeys are sensitive to the spatial arrangement of oriented visual stimuli. These neurons respond to a narrow range of orientations of bars or gratings presented within a confined region of the visual field, termed the ‘classical receptive field (CRF)’<sup>1,2</sup>. By definition, stimuli that are placed within the CRF of a given neuron result in vigorous responses, and stimuli presented alone and entirely outside the CRF do not evoke responses. However, if stimuli are presented simultaneously both within and outside the CRF, the extra-CRF stimuli can modify the responses evoked by the CRF stimuli<sup>3,4</sup>. The nature of the modification varies among neurons<sup>5–8</sup>. Surrounding bars or gratings oriented parallel to those presented within the CRF suppress the responses evoked by the CRF stimulus (‘iso-orientation’ suppression) to varying degrees. In contrast, surrounding bars or gratings oriented orthogonal to those presented within the CRF can produce a variety of ‘cross-orientation’ effects ranging from suppression to facilitation; some orthogonal stimuli have no cross-orientation effect. We refer to the orientation-dependent effects of surround modification as ‘contextual modulation’.

Previous studies have demonstrated that the properties of contextual modulation depend critically on local connections<sup>9</sup>, but there has been no attempt to systematically predict the relationship of contextual modulation to the entire orientation map. Neurons with similar orientation preferences are locally clustered in orientation columns or domains<sup>10,11</sup>. Groups of orientation domains with a full set of orientation preferences converge at a point; such groups are arranged in a pinwheel-like manner around this central point, the ‘pinwheel center’ (PWC), across the cortical surface<sup>12,13</sup>. The preferred orientations of domains change smoothly around PWCs, but change abruptly across PWCs. Local axons of both excitatory and inhibitory neurons radiate laterally by ~500 μm with no respect for the orientation preferences of neighboring domains<sup>14,15</sup>. Therefore, near the PWC, local axons may connect neurons with a variety of orientation preferences (see ref. 16 for other possibilities); in contrast, in regions farther away from the PWC, local axons connect neurons with more uniform orientation preferences<sup>14,17</sup>.

Given the evidence that local axons contribute to contextual modulation<sup>9,18,19</sup>, we hypothesized that the properties of contextual modulation depend on the locations of neurons within the orientation preference map. Investigation of this issue addresses the functional architecture of contextual modulation in V1, and is a critical step toward understanding the neuronal mechanisms for computation of curvature, corners, and



non-Cartesian gratings (concentric, radial, and hyperbolic patterns) at the next stages of the cortical pathway<sup>20</sup>. We tested our hypothesis using a computational approach. We first obtained the orientation preference maps of macaque V1 using optical imaging of intrinsic signals, and extensively analyzed the spatial distribution of orientation domains in concentric annular regions across the maps. This analysis revealed that the cortical regions farther away from PWCs contain more biased orientation distributions than those near PWCs; the orientation preference bias varied from iso- to cross-orientation as distance increased from the center of the annulus. Incorporating the features of the orientation map, we constructed a computational model of V1 that includes local recurrent connections. The computer simulations showed that strengths of both orientation tuning and contextual modulation gradually decreased as a function of a neuron's proximity to the PWCs. These results support the hypothesis that contextual modulation is a function of location within the orientation preference map. Furthermore, our simulations showed a clear difference between the strengths of orientation tuning and contextual modulation at the PWC, where there was some degree of orientation tuning but much reduced or absent contextual modulation. This finding led to a second new hypothesis, namely, that signals for local orientation are detected by neurons at or near the PWC, whereas signals for local orientation differences are detected by neurons distant from the PWC.

## Results

**Network model using the orientation preference map.** We constructed a simple model cortex, and simulated the responses of neurons at different cortical locations to the orientations of gratings. The stimuli were presented either as a single oriented stimulus within the CRF, or as a combination of oriented stimuli, some completely

within and some entirely outside the CRF (Fig. 1 and see Methods). Our model was based on the spatial distributions of orientation domains in the orientation preference map (Fig. 2, Supplementary Fig. S1), and assumed a spatially isotropic pattern of local recurrent connections between neurons<sup>14,17,21</sup>, including either monosynaptic connections (Supplementary Fig. S2a) or polysynaptic connections (Supplementary Fig. S2b). In our modeling approach, we precisely controlled the feedforward input from the map, restricting the neuronal interactions to local recurrent connections<sup>21</sup>, and computed the neuronal activity at all locations evenly across the surface of V1. In our model, the strength of feedforward input to a neuron was a function of the cosine of the angle between the preferred orientation at the neuron and the orientation of the stimulus. The responses of a model neuron are calculated by spatial summation over the areas of orientation domains, weighted by both the strength of feedforward input to the neuron and the strengths of connections with all other neurons.

**Orientation distributions around a single point at different map locations.** In the orientation maps of macaque V1, the distribution of orientation-selective domains around a single point on the cortex (e.g., plus sign in Fig. 2a,b) systematically varied with the distance from the nearest PWC (e.g., nearby black dot in Fig. 2a, arrow in Fig. 2b) to the point. We quantified the frequency distributions of preferred orientations of domains around each cortical site in the map, in order to examine the orientation information provided from near-field regions across the map via local interactions<sup>9</sup>. Each region of interest (ROI), up to 1 mm in radius, was divided into 20 concentric annular regions of equal width (Fig. 2b). The orientation distribution of pixel counts within these annular regions (a set of vertically ordered strips in the upper panels of Fig. 2c) gradually varied with the radius of the annular region.

Orientation bias in each annular region varied gradually, depending on two spatial parameters. The first parameter was the radius of the region (the abscissa of each panel in Fig. 2c, ranging from 0 to 1 mm; statistical significance: sign tests,  $P < 0.0025$ , red asterisks in Fig. 2c); the second was the location of the region, defined by the distance from the nearest PWC to the center of the region (panels from left to right in Fig. 2c). In ROIs distant from PWCs, especially more than 0.04 mm from PWCs, the orientation distribution index (ODI, see Methods) fluctuated remarkably over the full range of radii of annular regions within that ROI (Fig. 2c, lower row, left four panels). In annuli with smaller radii ( $< 0.25$  mm), all the ODIs were significantly positive, indicating the dominance of domains with preferred orientations within  $\pm 7.5^\circ$  (iso-orientation) of the preferred orientation of the neuron centered in the ROI. In annuli with intermediate radii (0.25–0.55 mm), all the ODIs were significantly negative, indicating the dominance of orientation domains with preferred orientations within  $90 \pm 7.5^\circ$  (cross-orientation) relative to the preferred orientation of the neuron at the ROI center. In annuli with larger radii (0.65–0.85 mm), all the ODIs were again positive. In contrast, in ROIs located at or near PWCs ( $< 0.04$  mm from PWCs), domains with different preferred orientations were almost equally distributed in most annular regions (Fig. 2c, lower row, rightmost panel). In annuli with radii of 0.45–1 mm, most ODIs were not significantly different from zero, but in annuli with smaller radii ( $< 0.45$  mm), the ODIs were significant (sign tests,  $P < 0.0025$ , red asterisks in Fig. 2c). All four monkeys (monkeys A–D) exhibited very similar patterns of spatial distribution of preferred orientations (Supplementary Fig. S1). Given the assumption that neurons have spatially isotropic synaptic connections, we suggest that a neuron receives input from surrounding neurons in a manner that varies depending both on the radius of the surrounding region from which the input is received and on the neuron's cortical location, defined by the distance from the nearest PWC.

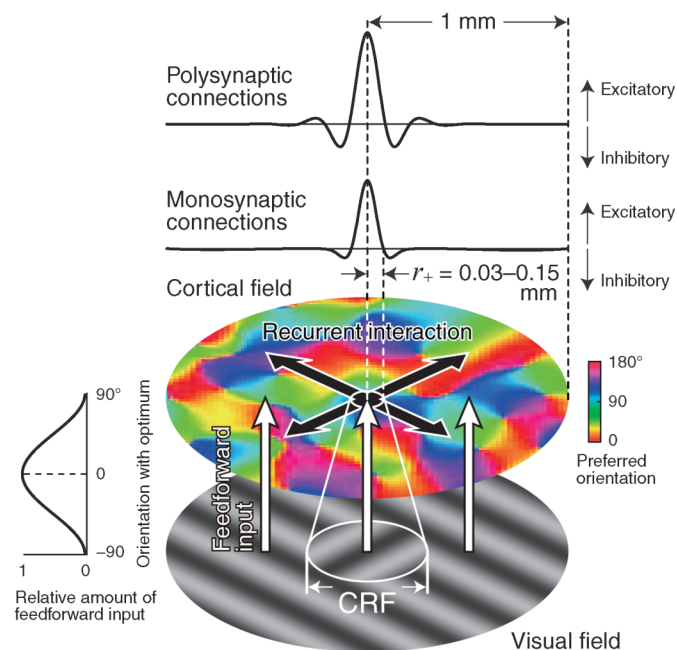


**Figure 1 | Overview of the model network.** The model neurons in the cortical field receive feedforward input from visual stimuli (white arrows). The amount of feedforward input received by a given neuron is determined based on the difference between the neuron's preferred orientation and the stimulus orientation (left panel). The white circle in the visual field illustrates the classical receptive field (CRF). The model neurons activated by the feedforward input interact with one another (black arrows) through local recurrent connections, either monosynaptic or polysynaptic (top two panels). A size parameter for the model connections,  $r_+$ , represents the extent of local excitatory interactions (white circle in the cortical field).

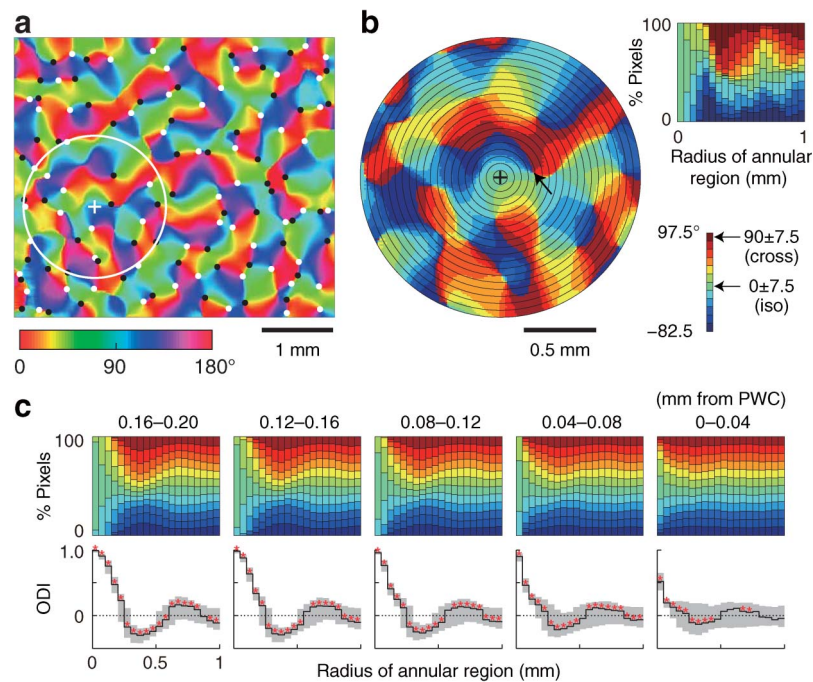


**Figure 2 | Spatial distribution of orientation preferences in monkey V1.** (a) Orientation preference map obtained by optical imaging. Color scale at the bottom left shows preferred orientations in degrees. White and black dots indicate clockwise and counterclockwise pinwheel centers (PWCs), respectively. The white circle represents an example of a region of interest (ROI), and the plus sign indicates the center of the ROI. (b) Magnified view of ROI, consisting of 20 concentric annular regions whose radii vary at 0.5 mm intervals (black circles). Color scale at bottom right shows the range of preferred orientation relative to the preferred orientation at the ROI center (plus sign). The top right panel shows the orientation population within the ROI as a function of annular region radius. (c) Variation of orientation populations in ROIs across the PWC. The imaged area ( $4.5 \times 3.9 \text{ mm}^2$ ) was scanned by shifting a circular ROI, and the data were pooled into five groups according to the distance between the ROI center and the nearest PWC: 0–0.04 to 0.16–0.20 mm from the PWC. Top row, orientation populations obtained from the median of pooled data in each group plotted as a function of annular region radius. Bottom row, the orientation distribution indices (ODIs) plotted as a function of annular region radius. Solid lines and gray areas indicate the median ODI and the range from 25th to 75th percentiles of ODIs, respectively. The ODIs in many regions differ significantly from zero (red asterisks,  $P < 0.0025$ ). Data for all monkeys are in **Supplementary Fig. S1**.

**Predicted orientation tuning at different map locations.** To calculate orientation-tuning curves at different map locations, we first simulated the responses of each neuron to oriented stimuli, across the orientation preference map (Fig. 1). Each stimulus was presented within the CRF of a specific neuron, and we considered contributions from direct monosynaptic connections between the given neuron and its surrounding neurons. The predicted orientation tuning curves showed bell-shaped profiles, with slopes that varied with distance from PWCs (Fig. 3a). Neurons farther away from PWCs ( $> 0.04 \text{ mm}$ ) showed sharper orientation tuning than those near PWCs. The median orientation selectivity indices (OSIs, see **Methods**) were 0.41 and 0.23, respectively, for neurons in 0.04–0.08 mm from PWC and neurons within 0.04 mm from PWC. The median orientation tuning widths (half-widths of tuning at half-height, HWHHs) were  $48^\circ$  and  $58^\circ$ , respectively, for neurons in 0.04–0.08 mm from PWC and neuron within 0.04 mm from PWC. The OSIs decreased, and the HWHHs increased, for neurons located closer to the PWCs (Fig. 3b). Both OSIs and HWHHs exhibited markedly broader distributions near PWCs (bottom histograms of Fig. 3b; see also **Supplementary Figure S2c** of ref. 16; see also refs. 22,23). This is not to say that a neuron at the PWCs has no orientation preference; instead, the simulation results indicate that neurons near PWCs have weaker, but still significant, orientation tuning. The OSIs remained smaller, and the HWHHs remained greater, for neurons near PWCs than for neurons distant from PWCs, over the range of the size parameter ( $r_+$ , the extent of local excitatory interactions; see Fig. 1) of the model connections (Fig. 3c). The variations in OSI and HWHH as functions of

distance from PWC are thus insensitive to changes in the size parameter of the model connections.

**Predicted contextual modulation at different map locations.** We next simulated neuronal responses of our model cortex to contextual stimuli. These stimuli were presented as circular patches of bipartite concentric gratings; the orientation of the center grating matched the neuron's preferred orientation, and the surrounding grating had a varying orientation (Fig. 1). Because the stimuli were assumed to extend beyond the CRF of a neuron, we needed to consider the contribution of indirect polysynaptic connections that link neurons in wider regions, in addition to the contribution of direct monosynaptic connections. To compare these contributions, simulations were performed separately for models of monosynaptic and polysynaptic connections.

The predicted responses of neurons to the contextual stimuli exhibited inverted bell-shaped tuning curves (Fig. 4a), as reported earlier for neurons in cat and monkey V1<sup>4–8</sup>. The model neurons responded minimally when the stimulus orientation in the surround was identical to that in the center (at  $0^\circ$  in Fig. 4a). Sharper tuning curves were obtained from neurons farther away from PWCs, whereas almost flat curves were obtained from those near PWCs. At each cortical location, the tuning curve generated by the polysynaptic model was sharper than that by the monosynaptic model. For a quantitative comparison, we calculated the contextual modulation index (CMI), which is defined by the response contrast between iso- and cross-orientation extra-CRF stimuli (see **Methods**). Larger absolute values of CMI reflect stronger surround modulation; positive

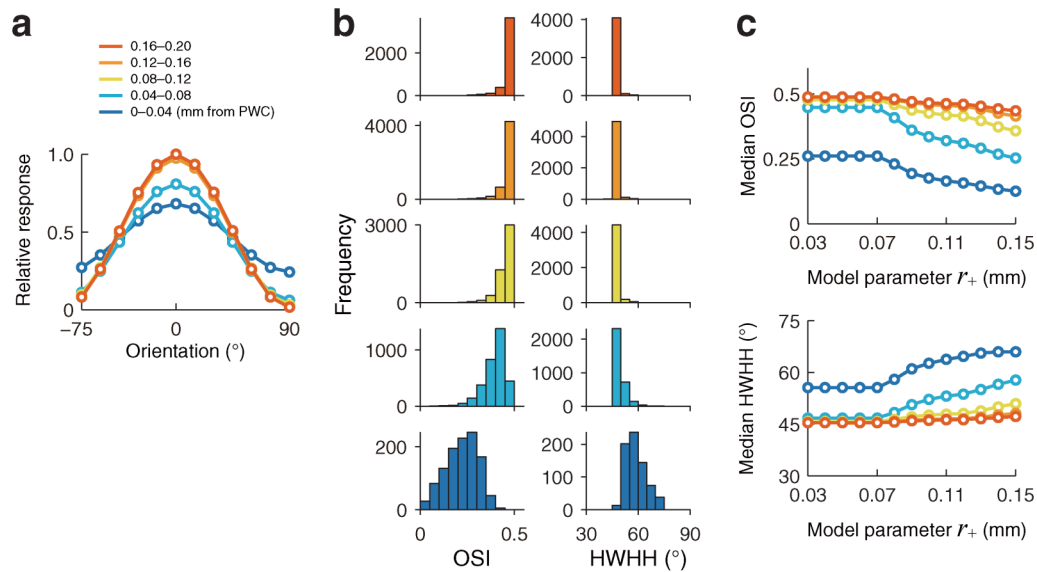


**Figure 3 | Predicted orientation tuning as a function of distance to PWCs.** The colors of the curves represent the map location as a function of distance from the nearest PWC. (a) Typical results of orientation tuning curves. Responses to an oriented stimulus within a neuron's classical receptive field (CRF) were calculated according to results in Fig. 2c, using a model cortex with monosynaptic connections defined by a Mexican hat-shaped function (see **Methods** and **Supplementary Fig. S2a**). The relative response amplitudes were obtained by dividing by the maximum response amplitude of neurons in regions 0.16–0.20 mm away from the PWC. The spatial extent of the connections was adjusted by a parameter representing the radius of the border between excitatory connections and inhibitory connections ( $r_+$ ). Here,  $r_+$  is set to 0.08 mm. (b) Distribution of orientation selectivity indices (OSIs) (panels in left column) and half-width of tuning at half-height (HWHH) (panels in right column) for 5 ranges of distances from PWCs. The color conventions are the same as those in (a). Both OSI and HWHH are measures of orientation tuning strength. For each neuron at the center of an ROI, these metrics were calculated from responses to stimuli within its CRF. The response to an oriented stimulus was computed using individual orientation populations, such as at the top right on Fig. 2b. The histograms of OSIs and HWHHs, grouped by distance from the PWC. (c) The variations in the median OSI (upper panel) and the median HWHH (lower panel) as a function of size parameter  $r_+$ . The colors of curves correspond to those in (a).

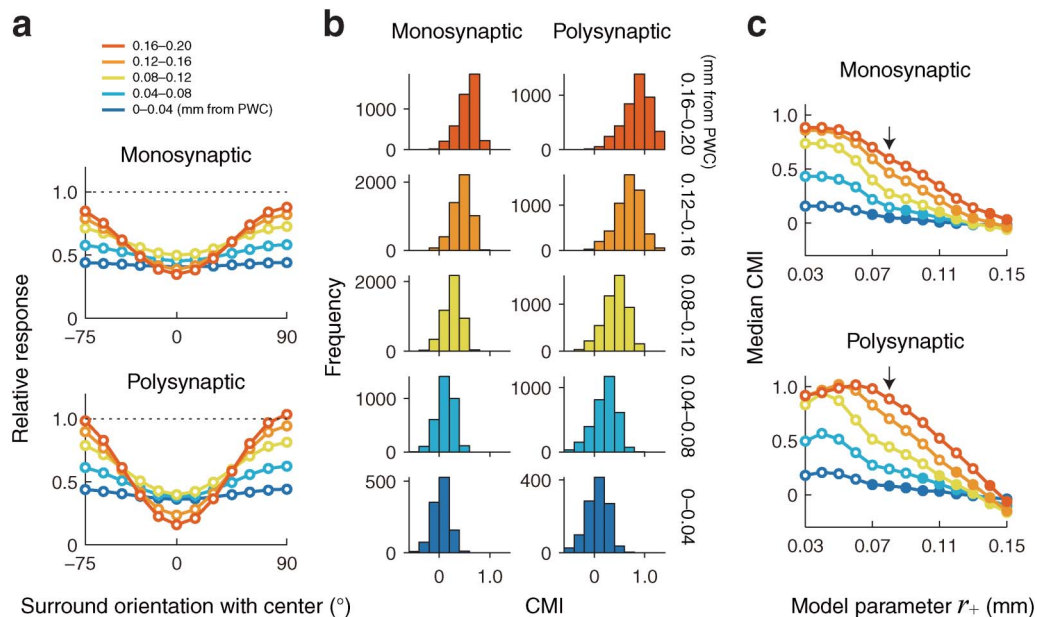


**Figure 4 | Predicted contextual modulation as a function of distance to PWCs.** Responses to an oriented stimulus outside the CRF, presented simultaneously with the preferred-orientation stimulus within the CRF, were calculated according to results shown in Fig. 2c and a model cortex with monosynaptic or polysynaptic connections. (a) Contextual modulation curves calculated for monosynaptic and polysynaptic connections (size parameter  $r_+ = 0.08$  mm). The polysynaptic connections were calculated theoretically from the monosynaptic connections (see **Methods** and **Supplementary Fig. S2**). The colors of the curves represent the distance from the nearest PWC. (b) Distribution of the contextual modulation indices (CMIs) for 5 ranges of distances from the nearest PWCs (see (a) for the color code). The CMI is a measure of the strength of contextual modulation, defined by the contrast between responses to iso- and cross-orientation extra-CRF stimuli. Each CMI was calculated by responses to stimuli within and outside the CRF at each neuron, centered on each ROI individually, in a manner similar to Fig. 3a. (c) Median CMI as a function of size parameter  $r_+$ . The filled circle indicates that the median CMI is close to zero: the OSIs have a value of zero between the 25th and 75th percentiles. The colors of curves correspond to those in (a). The arrows indicate the parameter value that maximizes the correlation coefficient between CMI and distance from PWC.



and negative CMI denote the preferences to cross-orientation and iso-orientation of surrounding stimuli. The CMI distributions showed similar profiles in the monosynaptic and polysynaptic models (Fig. 4b). Median CMI became gradually smaller with decreasing distance from the nearest PWC, and the CMI distributions for neurons at or near the PWC were centered at zero (bottom panels in Fig. 4b; filled circles in Fig. 4c). The CMI showed a strong positive correlation with distance from the PWC for both monosynaptic CMI (maximum  $r_s = 0.68$ ,  $P < 0.0025$ , Spearman's rank correlation at  $r_+ = 0.08$  mm; arrow in top panel, Fig. 4c) and polysynaptic CMI (maximum  $r_s = 0.67$ ,  $P < 0.0025$ , Spearman's rank correlation at  $r_+ = 0.08$  mm; arrow in bottom panel, Fig. 4c). For each distance group except for the group of 0–0.04 mm from the PWC, the median CMI generated by the polysynaptic model was larger than that by the monosynaptic model (compare left and right histograms in Fig. 4b). However, both monosynaptic and polysynaptic model connections showed that the CMI gradually decreased to approximately zero at PWCs, indicating that contextual modulation was absent or very weak at PWCs.

To understand how neurons detect orientation differences in contextual stimuli, we examined the responses of model neurons to iso- and cross-orientation contextual stimuli. The strength of iso-orientation suppression depended on the distance from the nearest PWC in a different manner than cross-orientation facilitation (compare Fig. 5a with Fig. 5b; see Methods for the definition of the strengths of iso-orientation suppression and cross-orientation facilitation). The correlation between the strength of iso-orientation suppression

and the distance from the PWC was sensitive to variation in the size parameter,  $r_+$ , of the model connections. For example, correlation coefficients greater than 0.5 (above dotted lines in Fig. 5) were obtained for a narrow range of the parameter, e.g.,  $r_+$  of 0.03–0.09 mm for monosynaptic connections, and  $r_+$  of 0.06–0.09 mm for polysynaptic connections (Fig. 5a). In contrast, the correlation between cross-orientation facilitation (see Methods) and distance from the PWC are relatively insensitive to variation in the size parameter (Fig. 5b). Correlation coefficients greater than 0.5 were seen for  $r_+$  of 0.03–0.15 mm for monosynaptic connections, and for  $r_+$  of 0.06–0.13 mm for polysynaptic connections. The strength of the correlation with distance from the PWC was more robust for cross-orientation facilitation than for iso-orientation suppression (compare dark orange plots to dark blue plots for the same size parameter  $r_+$  in Fig. 5b).

Our simulations demonstrated another important feature of contextual modulation, namely, that cross-orientation facilitation occurred only through polysynaptic connections (in particular, for a distance range of 0.08–0.20 mm away from the PWC; see gray areas in Fig. 6a, top three panels). Monosynaptic connections did not enhance the responses of model neurons more than the strongest response to CRF stimuli (data not shown). Furthermore, facilitation occurred in a narrow range of the size parameter; only for  $r_+$  of 0.04–0.08 mm did more than 25% of simulated neurons show cross-orientation facilitation (Fig. 6b). The facilitation at a given neuron decreased as the neuron neared the PWC under simulations with size parameter  $r_+$  of 0.06–0.10 mm. We suggest that

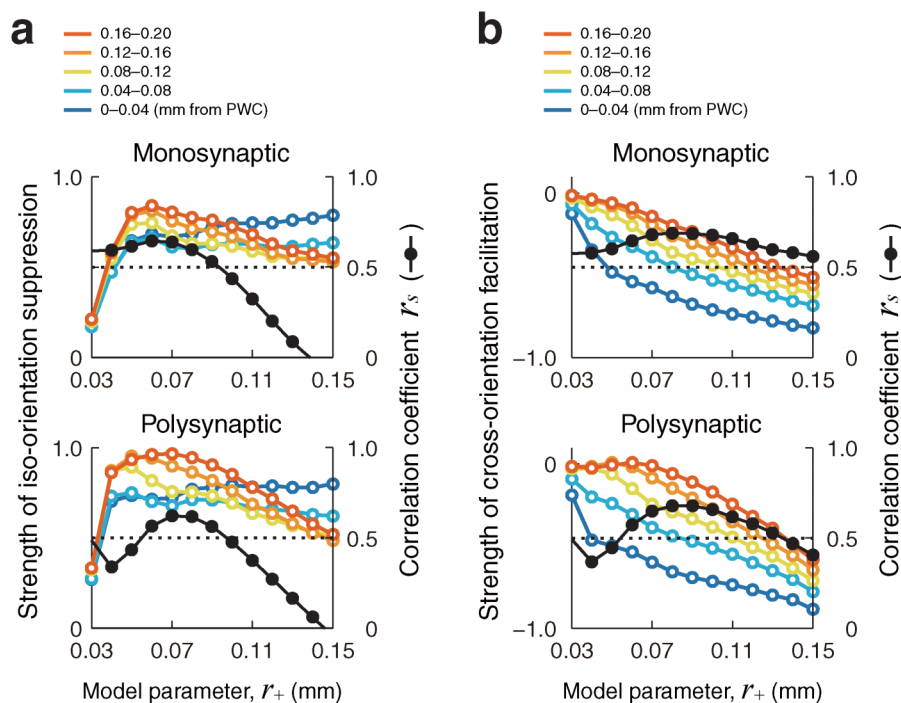


**Figure 5 | Iso-orientation suppression and cross-orientation facilitation calculated for different parameters of monosynaptic and polysynaptic connections.** (a) The strength of iso-orientation suppression (the colored curves, the left vertical axis) and the correlation coefficient between the suppression strength and the distance from the PWC (the black curve, the right vertical axis), plotted as a function of a size parameter that determines the spatial scale of local recurrent connections. The strength of iso-orientation suppression was calculated by subtracting responses to iso-orientation stimuli presented both within and outside the CRF (plots at  $0^\circ$  in Fig. 4a) from the response to preferred orientation stimuli presented alone within the CRF (dotted line in Fig. 4a). Then, the strength is normalized against the response to preferred-orientation stimuli within the CRF alone (see Methods). (b) The strength of cross-orientation facilitation (the colored curves, the left vertical axis) and the correlation coefficient between the facilitation strength and the distance from the PWC (black curve, right vertical axis) are plotted as a function of the size parameter. The strength of cross-orientation facilitation was calculated by subtracting the response to preferred-orientation stimuli presented alone within the CRF (dotted line in Fig. 4a) from responses to cross-orientation stimuli presented both within and outside the CRF (plots at  $90^\circ$  in Fig. 4a). Then, the strength is normalized against the response to preferred-orientation stimuli presented alone within the CRF (see Methods).



location-dependent cross-orientation facilitation was evoked only by polysynaptic connections with a particular projection size, under a mechanism involving local recurrent connections.

### Time course of orientation tuning and contextual modulation.

Our simulations thus far were performed using a single-iteration approach based on models with either monosynaptic or polysynaptic connections. In theory, the model with polysynaptic connections includes effects of multiple iterations. However, the polysynaptic input to a neuron in our model is computed simply by summation of outputs from surrounding neurons through iterated calculations of neuronal interactions. Therefore, our model explains only the effects of spatial integration, but not the temporal change in surround effects<sup>24</sup>. To understand the time course of orientation tuning and contextual modulation, we performed simulations based on the case in which each neuron receives both stationary feedforward input and recurrent input from surrounding neurons in the preceding iterations. The neuronal response amplitudes obtained by this simulation were altered just after one iteration, and saturated after 10 or more iterations (top two panels in Fig. 7). Far from the PWC, the profiles of tuning curves for both orientation selectivity and contextual modulation gradually became sharper with time (orange lines in two panels of the third row in Fig. 7). Near the PWC, each tuning curve showed little change between one iteration and 20 iterations (blue lines in two panels of the third row in Fig. 7). Furthermore, the tuning curves after one iteration and 20 iterations are qualitatively similar to the tuning

curves calculated by models with either monosynaptic or polysynaptic connections (compare third and fourth rows in Fig. 7a and 7b). Thus, we suggest that the tuning curves obtained from the monosynaptic connection model varied to those obtained from the polysynaptic connection model continuously with time.

### Effects of CRF scatter on orientation tuning and contextual modulation.

Neighboring V1 cells have considerable scatter in their receptive fields, roughly of the order of the size of the average receptive field<sup>25–27</sup>. We examined the influence of this distortion of visuotopy on predicted orientation tuning and contextual modulation. We added a term for CRF scatter to our model, and calculated the indices of orientation tuning and contextual modulation using the size parameter  $r_+ = 0.08$  mm (Fig. 8a), as we did for Figs. 3, 4, and 5. Note that the CRF radius corresponds to 0.1 mm on the model cortex. In this simulation, the CRF scatter was modeled by assuming two-dimensional normal distributions of various degrees of CRF center displacement (Fig. 8b). When the CRF scatter is within the range of CRF size (standard deviation of the CRF center displacement  $\sigma < 0.1$  mm, leftward from the dotted line in Fig. 8a), each index showed almost the same value as that obtained from the model lacking CRF scatter (compare top two panels in Fig. 8a with plots at  $r_+ = 0.08$  mm in Fig. 3c; compare third and fourth panels in Fig. 8a with plots at  $r_+ = 0.08$  mm in Fig. 4c; compare fifth and sixth panels in Fig. 8a with plots at  $r_+ = 0.08$  mm in Fig. 5a; compare bottom two panels in Fig. 8a with plots at  $r_+ = 0.08$  mm in Fig. 5b). When the CRF scatter is outside the range of CRF size, this trend of CMIs inverts rapidly. Thus, introduction of CRF scatter smaller than the CRF size into the model did not change our findings regarding OSI, HWHH, CMI, iso-orientation surround suppression, or cross-orientation surround facilitation; results were similar to those obtained from the model lacking CRF scatter.

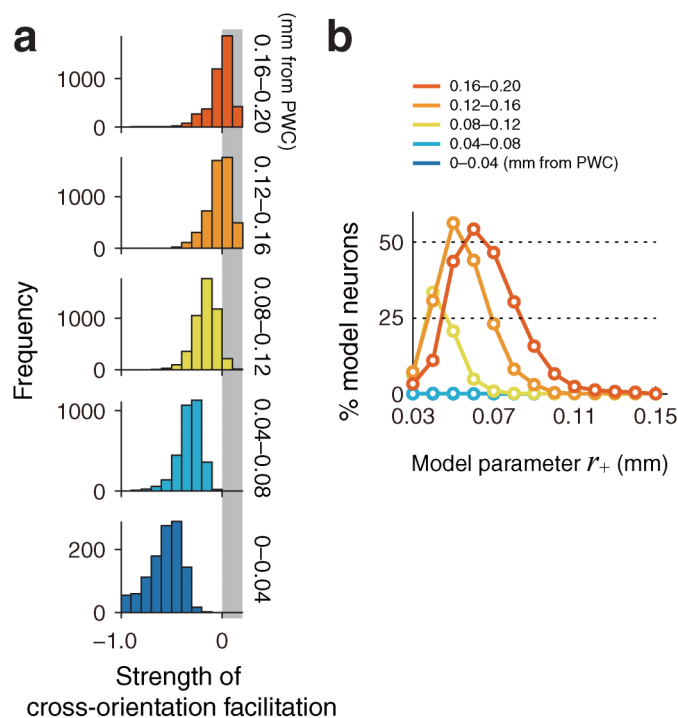


**Figure 6 | Cross-orientation facilitation with different size parameters, for a model with polysynaptic connections.** (a) Distributions of the strengths of cross-orientation facilitation for different distances from the nearest PWC (see (b) for the color codes). The strength of cross-orientation facilitation was calculated by subtracting the response to preferred-orientation stimuli presented alone within the CRF (dotted line in Fig. 4a) from the response to preferred-orientation stimulus within the CRF presented in conjunction with cross-orientation stimuli outside the CRF (plots at  $90^\circ$  in Fig. 4a). The gray area indicates the effect of facilitation. (b) The percentage of facilitated ROIs as a function of the parameter for the spatial scale of local recurrent connections,  $r_+$ . The colors of curves represent the distance from the nearest PWC.

### Discussion

The functional specificity of PWCs is not well understood at the neuronal level, although orientation pinwheels have been thought of as the basic units of orientation maps<sup>28</sup>. We simulated a local recurrent network overlaid on the orientation map, and demonstrated that the orientation processing capability gradually decreases near the PWCs. In our simulations, neurons near the PWC showed weak but detectable (and more broadly distributed) tuning to orientation of stimuli covering their CRF alone, and exhibited weak contextual modulation by extra-CRF stimuli. Two previous experimental studies have reported a smooth change in contextual modulation across V1, one for local regions extending within  $1\text{ mm}^9$  and the other for larger regions extending beyond  $1\text{ mm}^{29}$ . To the best of our knowledge, no experiments have rigorously investigated contextual modulation at PWCs. Based on our results, we suggest that neurons at PWCs have a stable orientation tuning regardless of the complexity of a visual scene, and are truly specialized for discrimination of local orientations within their CRFs. This interpretation is different from the classical hypothesis that neurons at PWCs are specialized for processing surface textures<sup>30</sup>. We also suggest that neurons distant from PWCs change their responses to their preferred orientations according to the complexity of a visual scene. Therefore, we propose a new hypothesis regarding the functional architecture of V1: information about stimulus orientation within a local visual field is faithfully processed at and near PWCs, and contextual information is processed at regions that are more distant from PWCs.

In our model, we considered the differences in contextual modulation between two systems of neuronal connections, i.e., monosynaptic and polysynaptic connections, using a single-iteration approach; we also examined such differences over a time course in a multiple-iteration approach. For neurons near the PWCs, the contextual modulation stays weak. For neurons distant from the PWCs,

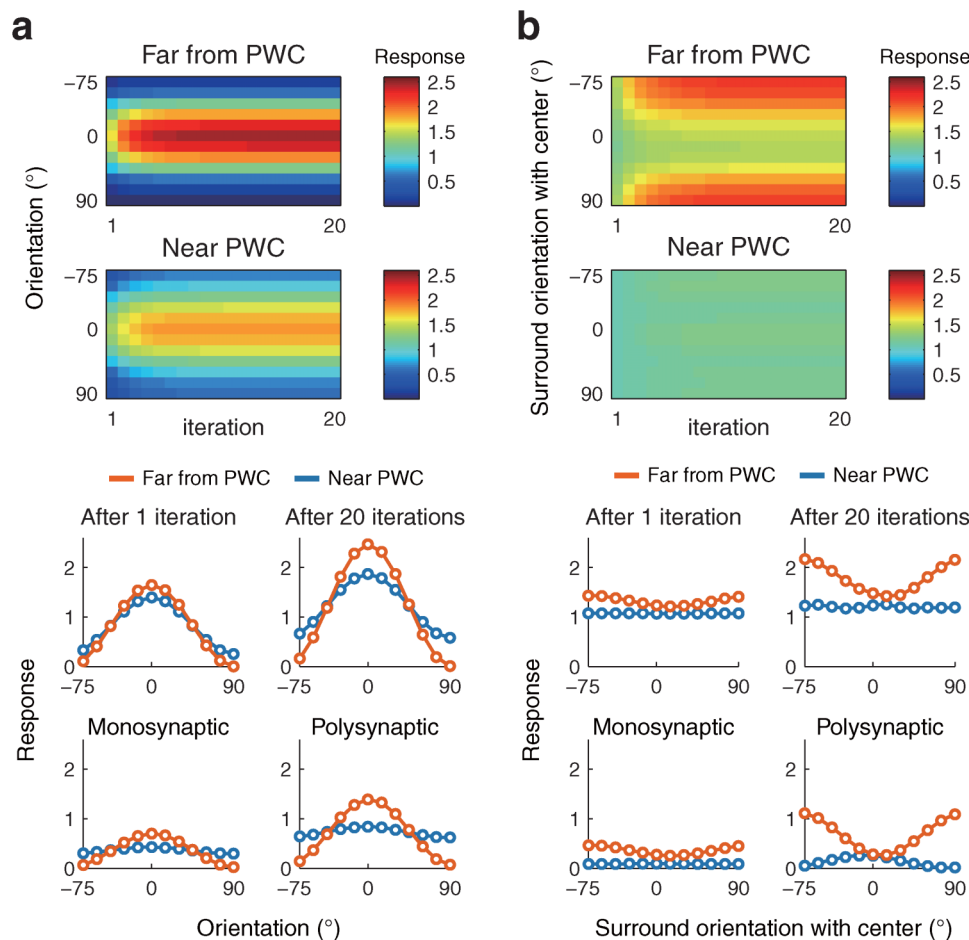


**Figure 7 | The time course of the orientation tuning and the contextual modulation with stationary inputs.** Every model neuron continuously receives feedforward input from the stimulus (a, for a center grating alone; b, for center and surrounding gratings), and also receives recurrent input from surrounding neurons derived from the preceding iterations. The time courses of responses of two individual neurons are shown in top two panels. The tuning curves are shown for one iteration (left panel of the third row) and for 20 iterations (right panel of the third row). For comparison, the tuning curves calculated by single-iteration simulations using models with monosynaptic or polysynaptic models are shown (bottom row).

contextual modulation gradually became stronger with time; and eventually, cross-orientation facilitation is evoked. Our results indicate that neurons distant from PWCs may emphasize information about ‘T-junctions’, where two orthogonally oriented contours come together, via polysynaptic connections. To understand the time course of contextual modulation in more detail, our model will need to be modified to include additional mechanisms, including feedback connections that can shape surround effects<sup>31</sup>, and pattern adaptation that affects interactions between neurons tuned to orthogonal orientations<sup>32</sup>.

The sharpness of stimulus orientation tuning at PWCs has been a subject of some controversy. We observed broader orientation tuning near the PWCs; this is consistent with recent studies using multi-electrode array recordings in conjunction with optical imaging in both cats and monkeys<sup>22</sup>, as well as studies using two-photon calcium imaging<sup>16</sup>. Other earlier studies reported a uniform distribution of orientation tuning of neuronal spike responses across the orientation map; that is, neurons near the PWCs are tuned to orientation as sharply as those away from PWCs<sup>23,33–35</sup>. Our simulation results on both OSIs and HWHs showed that tuning strength varies widely among neurons near the PWCs (Fig. 3b; see also Ref. 16). Studies that rely on physiological experiments with small sample sizes may overlook the difference in tuning strengths between neurons near PWCs and distant from PWCs.

In our approach, we simulated cortical responses by applying a neuronal interaction model to the experimentally obtained map of

preferred orientation of neurons in monkey V1. In general, the preferred orientations calculated from the optical-imaging data are thought to include all the effects of bottom-up, lateral, and top-down visual processing. However, some studies using the technique of cooling the visual cortex<sup>36</sup> or the GABA agonist muscimol<sup>37</sup> have shown that the preferred orientations of naive neurons match the preferred orientations of neurons with feedforward input only. We therefore believe that the orientation map of V1 obtained by optical imaging correctly reflects the preferred orientations of neurons derived solely from feedforward input.

In order to estimate extra-CRF contextual modulation, we analyzed the orientation distribution in each annular region, at intervals of 0.05 mm, up to a 1 mm radius. This analysis revealed that for a given neuron, the domains corresponding to the preferred orientation are dominant with the circular region of 0.25 mm and the annular region of radius 0.65–0.85 mm; domains corresponding to the orthogonal orientation are dominant in the annular region of radius 0.25–0.55 mm (Fig. 2 and Supplementary Fig. S1). The spatial distribution of domain clusters of orthogonal and preferred orientations in regions that are distant (> 0.25 mm) from a given neuron is a key factor governing the variation in contextual modulation as a function of map location. This type of orientation bias in distant regions has not been previously reported. Earlier studies estimated the local input tuning by analyzing the spectrum of preferred orientations within an entire region of radius greater than 0.2 mm<sup>22,33,38</sup>.

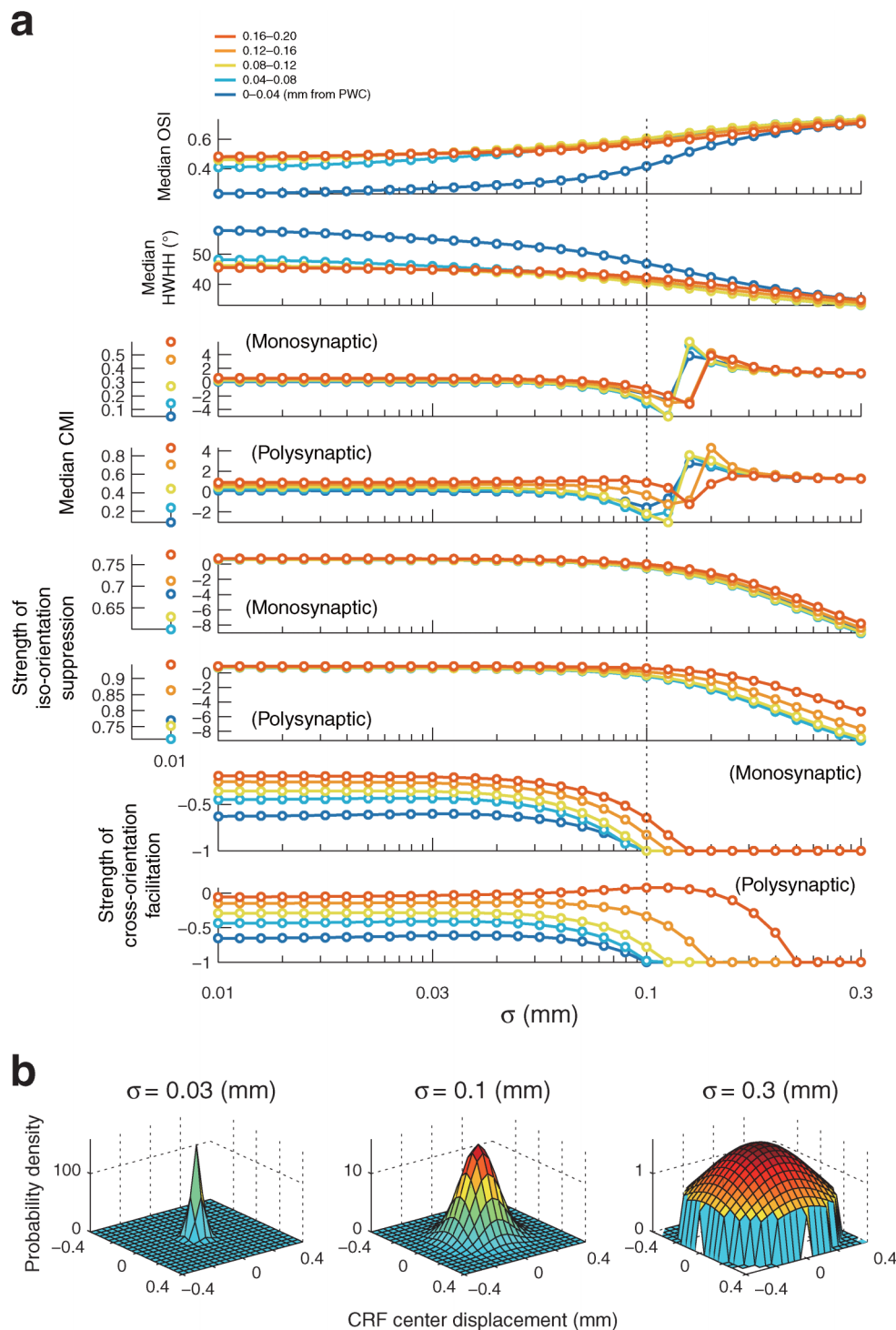


**Figure 8** | The influence of CRF scatter on orientation tuning and contextual modulation. (a) The medians of OSI, HWHH, CMI, the strength of iso-orientation suppression and the strength of cross-orientation facilitation are plotted against the standard deviation of CRF center displacement  $\sigma$ . Dotted line indicates the  $\sigma$  that corresponds to the CRF size. (b) Profiles of a hypothetical distribution of various degrees of CRF center displacement.

We simulated the strength of contextual modulation by designing a model that incorporates short-range recurrent connections but not long-range recurrent connections. We believe that the exclusion of the long-range connections is appropriate for our simulations (Fig. 1). We defined the CRF size so that the grating maximizes the responses of a neuron, based on the spatial extent of excitatory connections of the model, e.g., the CRF radius of our model is 0.1 mm with size parameter  $r_+ = 0.08$  mm. The radius of the excitatory connections ( $r_+$  in the model) ranged from 0.03 to 0.15 mm in

our simulations, matching the region in which excitation dominates, as determined by scanning laser photostimulation in tangential brain slices<sup>21</sup>. When the radius of the receptive field with feedforward input alone is expressed by  $R_{FF}$ , the diameter of the CRF can be calculated as  $D_{CRF} = 2(R_{FF} + r_+)$  (Supplementary Fig. S3). Hence, under a simple assumption (no distortions of visuotopy), the distance between a given neuron activated by the center stimulus and a surrounding neuron activated by surround stimulus can be estimated as  $D_{CRF} - r_+$ . The diameter of the CRF is 0.33° in monkey





V1 at  $\sim 6^\circ$  eccentricity of visual field representation<sup>39</sup>; the cortical magnification factor is 2.3 mm/degree in monkey V1 at  $5^\circ$  eccentricity<sup>27</sup>. The visual stimuli that we used in optical imaging were centered at  $5^\circ$  eccentricity. If we place the surrounding stimulus just outside the CRF of a given neuron, the center-to-center spacing between the feedforward receptive field of the neuron and that of the surrounding neuron within the surrounding stimulus on the V1 cortex can be calculated as follows:

$$0.33 \text{ (degree)} \times 2.3 \text{ (mm/degree)} = [0.03 \sim 0.15] \text{ (mm)} \\ = [0.61 \sim 0.73] \text{ (mm)}.$$

These values are smaller than the extent of long-range horizontal connections ( $> 1$  mm). Thus, the stimuli in our simulations are not influenced by long-range interactions.

The idea that short-range recurrent connections contribute to contextual modulation has been suggested by experiments<sup>9,18,19</sup> and simulations<sup>40,41</sup>. However, in order to understand how stimuli larger than those considered here modulate the neuron's activity, other mechanisms involving widespread axonal projections, such as long-range connections in V1<sup>42</sup>, should also be considered. Most long-range lateral connections are excitatory ones between neurons with similar orientation preferences, separated by several millimeters<sup>43,44</sup>, and cannot directly drive iso-orientation suppression. In order to explain the conversion of long-range excitation to contextual suppression, a local circuit mechanism involving inhibitory interneurons was proposed<sup>45</sup>. Radially symmetric short-range inhibitory connections have been observed in physiological experiments<sup>21,43</sup>. Therefore, iso-orientation surround suppression will be evoked in the iso-orientation domains distant from PWCs, and non-specific surround suppression will be evoked near PWCs. This reasoning is consistent with our results. Note, however, that involvement of an intracortical inhibitory mechanism in surround suppression has remained controversial because of potentially confounding evidence e.g., microiontophoretic application of a type-A GABA receptor antagonist, bicuculine methiodide, to cat V1 cells does not eliminate surround suppression<sup>46</sup>. The scheme described above also fails to explain cross-oriented surround facilitation. In order to further elucidate the mechanism of contextual modulation, future experiments should examine longer-range connections and characterize the relationship between a neuron's location and the spatial distributions of its connections.

The contextual modulation of a neuron by extra-CRF stimuli is related to the secondary processing of visual contours. We calculated the variation of contextual modulation effects, based on the configuration of the orientation map. Our results indicate that the brain effectively uses the orientation preference map for additional contextual processing. In order to more accurately investigate the specificity of the contextual modulation for cortical location, it will be necessary to perform both fine-scale mapping of orientation preference and fine-scale mapping of contextual modulation. The results and predictions of this study will provide a basis for future experimental studies of the monkey cortex, using state-of-the-art techniques such as two-photon laser microscopy<sup>16</sup>.

## Methods

All experimental procedures were approved by the animal experiment committee of Osaka University, in accordance with the guidelines of the National Institutes of Health (1996). The experimental procedures are described in detail elsewhere<sup>47</sup>.

**Animal preparation.** Four anesthetized monkeys (*Macaca fuscata*; body weight, 7.35–7.40 kg) were used. The monkeys were prepared for repeated recordings by an initial aseptic surgery under sodium pentobarbital surgical anesthesia. For optical imaging studies, monkeys were artificially ventilated through a tracheal cannula, and anesthetized with fentanyl citrate (0.035 mg/kg/h, Fentanest, Sankyo, Tokyo) and a mixture of isoflurane (1–3%) and nitrous oxide (70%). Body temperature was maintained at  $37\text{--}38^\circ\text{C}$ . End-tidal  $\text{CO}_2$  was maintained at  $4.0\text{--}4.5\%$ . Electrocardiogram, blood pressure and arterial oxygen saturation levels were continuously monitored throughout the experiment. Eyes were dilated and covered

with appropriate contact lenses. The monkeys were paralyzed with pancuronium bromide (0.02 mg/kg/h, i.v., Mioblock, Organon, Osaka) to prevent eye movements during optical imaging.

During duratomy, glycerol (0.2 g/kg/h, i.v., Chugai, Tokyo) was administered to prevent edema. We made a hole ( $10 \times 10$  mm) in a posterior segment of the skull above V1, and exposed a  $6 \times 6$  mm region of cortex by reflecting the dura. A thin, transparent silicone rubber sheet was placed over the exposed brain. The four sides of the sheet were slipped below the dura. The hole was covered with a transparent plastic plate and filled with 1% agar containing antibiotics (gentamicin sulfate, 0.5 mg/mL, Gentacin, Schering-Plough, Osaka) and adrenal cortical hormone (dexamethasone sodium phosphate, 0.1 mg/mL, Decadron, Banyu, Tokyo).

**Optical imaging.** Changes in light reflectance driven by neural activity ("intrinsic signals"<sup>48</sup>) were recorded from the surface of V1 under fentanyl citrate anesthesia. We first acquired an image of the vascular pattern of the cortical surface using band-pass filtered light at  $542.5 \pm 23$  nm. We then lowered the focal plane to  $600\text{--}800$   $\mu\text{m}$  below the cortical surface, and performed intrinsic signal recording using band-pass filtered light at  $628.3 \pm 9.6$  nm. Images were taken using a charge-coupled device camera (KP-MIE/K, Hitachi Denzhi, Tokyo) with a tandem-lens microscope, and digitized with a frame grabber board (Pulsar, Matrox, Quebec, Canada). The frame rate of recording was 24 Hz. To generate 'snapshots' at 0.5 s intervals, 12 sequential images were summed to create one image. We recorded a  $4.5 \times 3.9$  mm region of the cortical surface. The recorded images had a spatial resolution of  $320 \times 280$  pixels after binning. For each trial, data collection started 1 s before stimulus onset and continued for 8 s.

**Visual stimuli.** Visual stimuli were presented on a cathode-ray tube (CRT) monitor with the aid of a graphics system (VSG, Cambridge Research Systems, Rochester, England) and our own custom-made software. Screen refresh rate was 100 Hz. Stimuli were circular patches of drifting square wave gratings (spatial frequency: 1.5 cpd; temporal frequency: 4 Hz; size:  $10^\circ$  in diameter; Michelson contrast: 98.6%; orientation: 0, 22.5, 45, 67.5, 90, 112.5, 135, and  $157.5^\circ$ ; position: contra-lateral and lower visual field with the center of grating placed at an eccentricity of  $5^\circ$ ). The direction of drift was orthogonal to the orientation of the gratings. The duration of presentation was 3 s. The interstimulus interval was 25 s. Stimuli were presented monocularly by occluding one eye using a mechanical shutter. The stimulated eye was selected pseudo-randomly across trials. 30 trials were performed for each stimulus condition.

**Data analysis.** A single-orientation activity map was obtained by averaging the recorded images associated with a particular orientation of gratings. The generalized indicator functions method<sup>49</sup> was used to maximize the signal-to-noise ratio. The single-orientation map was smoothed using the  $9 \times 9$ -pixel convolution kernel with uniform pixel weighting. The preferred orientation  $\phi$  at pixel  $(i, j)$  was computed by vector averaging of signals at the pixel, using 4 orientations (Monkey A; Fig. 2) or 8 orientations (Monkeys B, C, D; Supplementary Fig. S1).

The position of a PWC was determined from the change of preferred orientations along the circumference of each pixel (3-pixel radius). The orientation change on the circumference was calculated by an index  $s_{ij}$  as follows:

$$s_{ij} = \Delta\phi(i, j+3; i+3, j) + \Delta\phi(i-3, j; i, j+3) + \Delta\phi(i, j-3; i-3, j) \\ + \Delta\phi(i+3, j; i, j-3),$$

where  $\Delta\phi(i_1, j_1; i_2, j_2)$ , ranging from  $-90^\circ$  to  $90^\circ$ , is the orientation difference between the pixel at  $(i_1, j_1)$  and the pixel at  $(i_2, j_2)$ . If the value of  $s_{ij}$  was equivalent to  $-180^\circ$  or  $180^\circ$ , the pixel at  $(i, j)$  was determined to be a candidate for a clockwise or a counterclockwise pinwheel center (PWC), respectively. The candidates were gathered into clusters; the maximum number of pixels that could belong to one cluster was 29. The coordinates of a PWC were obtained by averaging the positions of candidates in a cluster.

In order to acquire orientation distributions for a map location, pixels with similar orientation preference were counted within a circular region of interest (ROI) sliding across the orientation map. Each ROI was segmented into 20 regions of concentric annuli with radii varying at intervals of 0.05 mm. The orientation preferences of pixels were arbitrarily sorted into 12 groups,  $\Delta\Theta_k$  ( $k = -5, -4, \dots, 5, 6$ ), according to the orientation relative to the preferred orientation at the ROI center:  $15k - 7.5^\circ \leq \Delta\Theta_k < 15k + 7.5^\circ$  (Fig. 2b). To quantify the breadth of orientation distribution, we used the following orientation distribution index (ODI):

$$\text{ODI} = c(a^2 + b^2)^{1/2} / \sum_{k=-5}^6 \% \text{Px}(\Delta\Theta_k),$$

where

$$a = \sum_{k=-5}^6 \% \text{Px}(\Delta\Theta_k) \cos(2\overline{\Delta\Theta_k}), \quad b = \sum_{k=-5}^6 \% \text{Px}(\Delta\Theta_k) \sin(2\overline{\Delta\Theta_k}),$$

$$\overline{\Delta\Theta_k} = 15k^\circ \quad (k = -5, -4, \dots, 5, 6),$$

$c = 1$  if  $|\arctan(b/a)| \leq 90^\circ$ ,  $c = -1$  otherwise;  $\% \text{Px}(\Delta\Theta_k)$  is the percentage of pixels with  $\Delta\Theta_k$  (Fig. 2b, c). ODI values ranged from  $-1$  to  $1$ . Positive ODIs indicate



iso-orientation dominance and negative ODIs indicate cross-orientation dominance in the orientation distribution of an annular region.

**Connectivity models.** Based on physiological evidence<sup>21</sup> and theoretical models<sup>41,50–53</sup>, we chose a Mexican hat-shaped function for the local recurrent connections. We defined the Mexican-hat function as a two-dimensional Laplacian-of-Gaussian function (LGF) (Fig. 1, Supplementary Fig. S2a) on a continuous cortical field. The LGF between a neuron at a given site, which is set to the origin (0,0), and a neuron at another site (x,y) was represented by

$$\text{LGF}(x,y) = (1/(\pi\sigma^2))(1 - (x^2 + y^2)/(2\sigma^2)) \exp(-(x^2 + y^2)/(2\sigma^2)),$$

where  $\sigma$  is a size constant determined by  $\sigma = r_+/\sqrt{2}$ . The size parameter  $r_+$  is the radius of the excitatory core region of LGF.

Polysynaptic weights were calculated stepwise. First, activity  $a_0$  at an arbitrary site (x,y) of a cortical field just after excitation at a given site (0,0) was determined by the LGF itself:  $a_0(x,y) = \text{LGF}(x,y)$ . Next, activity  $a_1$  at (x,y) after receiving input monosynaptically was computed by convolving the preceding activity at the other sites  $a_0(x',y')$  with the LGF as follows:

$$a_1(x,y) = \iint \text{LGF}(x',y') \times a_0(x-x',y-y') dx' dy'.$$

Third, activity  $a_n$  at the site (x,y) after  $n$  iterations of activity propagation was computed by repeating the above calculation using the Fourier transform  $F\{\}$  and the inverse Fourier transform  $F^{-1}\{\}$  as follows:

$$F\{a_n(x,y)\} = F\{\text{LGF}(x,y)\} \times F\{a_{n-1}(x,y)\} = [F\{\text{LGF}(x,y)\}]^n,$$

$$a_n(x,y) = F^{-1}\{[F\{\text{LGF}(x,y)\}]^n\}.$$

Finally, the cortical point-spread function (PSF) of neuronal activity was calculated by summing field activations during iterations as follows:

$$\text{PSF}(x,y) = \sum_{n=1}^N a_n(x,y).$$

The number of iterations ( $N = 10$ ) was determined so that  $a_{N-1}(0,0) > 0.01 \times a_1(0,0)$  and  $a_N(0,0) < 0.01 \times a_1(0,0)$ . In calculation of the PSF, excitation and inhibition were repeated more than once with a decay in amplitude, whereas excitation and inhibition appear only once in calculation of the LGF (Supplementary Fig. S2b).

**Simulation.** The responses of a neuron to oriented stimuli inside and outside the neuron's CRF were simulated using a two-step process: integration of input and input-output transformation. The stimuli fed to the model were bipartite concentric gratings in which the orientations of the gratings were varied; the orientation of each grating is  $\theta_m = 15m^\circ$ ,  $m = -5, \dots, 6$ . The center disk with radius  $r_c$  corresponds to the CRF. The surrounding annulus alone did not evoke any response. The input to the neuron in the center from neurons in the annular region (mean radius:  $r_n = 0.05n - 0.025$  mm,  $n = 1, \dots, 20$ ; width:  $\Delta r = 0.05$  mm) through monosynaptic connections  $\Delta I^{\text{mono}}$  and that through polysynaptic connections  $\Delta I^{\text{poly}}$ , were respectively given as follows:

$$\Delta I^{\text{mono}}(r_n, \theta_m) = \sum_k \text{LGF}(x,y) \times (2\pi r_n \Delta r \times \%P_x(\Delta\Theta_k)/100) \times \cos(\overline{\Delta\Theta_k} - \theta_m),$$

$$\Delta I^{\text{poly}}(r_n, \theta_m) = \sum_k \text{PSF}(x,y) \times (2\pi r_n \Delta r \times \%P_x(\Delta\Theta_k)/100) \times \cos(\overline{\Delta\Theta_k} - \theta_m),$$

where (x,y) satisfies  $r_n = (x^2 + y^2)^{1/2}$ , e.g.,  $x = r_n$  and  $y = 0$ . The cosine functions at the far right of the right-hand sides of these equations represent the tuning curves for feedforward input. Next, the spatial integration of input  $I^{\text{conn}}$  is computed as follows:

$$I_{\text{cent}}^{\text{conn}}(\theta_{\text{cent}}) = \sum_{n=1}^c \Delta I^{\text{conn}}(r_n, \theta_{\text{cent}}) \text{ for a center grating alone,}$$

$$I_{\text{cent+surr}}^{\text{conn}}(\theta_{\text{cent}}, \theta_{\text{surr}}) = \sum_{n=1}^c \Delta I^{\text{conn}}(r_n, \theta_{\text{cent}}) + \sum_{n=c+1}^{20} \Delta I^{\text{conn}}(r_n, \theta_{\text{surr}})$$

for center and surrounding gratings,

where 'conn' corresponds to either 'mono' for monosynaptic connections or 'poly' for polysynaptic ones;  $\theta_{\text{cent}}$  and  $\theta_{\text{surr}}$  are the orientations of a center grating and those of a surrounding grating, respectively. Finally, the output  $R^{\text{conn}}$  is determined as follows:

$$R_{\text{cent}}^{\text{conn}}(\theta_{\text{cent}}) = f(I_{\text{cent}}^{\text{conn}}(\theta_{\text{cent}})) \text{ for a center grating alone,}$$

$$R_{\text{cent+surr}}^{\text{conn}}(\theta_{\text{cent}}, \theta_{\text{surr}}) = f(I_{\text{cent+surr}}^{\text{conn}}(\theta_{\text{cent}}, \theta_{\text{surr}})) \text{ for center and surrounding gratings,}$$

where  $f(I)$  is an input-output transfer function defined as  $0 (I < 0)$  or  $I (I \geq 0)$ .

When we considered the effect of CRF scatter, we revised our model as follows:

$$I_{\text{cent}}^{\text{conn}}(\theta_{\text{cent}}) = \sum_{n=1}^{20} P^{\text{cent}} \Delta I^{\text{conn}}(r_n, \theta_{\text{cent}}) \text{ for a center grating alone,}$$

$$I_{\text{cent+surr}}^{\text{conn}}(\theta_{\text{cent}}, \theta_{\text{surr}}) = \sum_{n=1}^{20} P^{\text{cent}} \Delta I^{\text{conn}}(r_n, \theta_{\text{cent}}) + \sum_{n=1}^{20} (1 - P^{\text{cent}}) \Delta I^{\text{conn}}(r_n, \theta_{\text{surr}})$$

for center and surrounding gratings,

$$P^{\text{cent}} = \frac{\iint_{\text{CRF} \cap \text{STM}_{\text{cent}}} G(\mathbf{x}, \boldsymbol{\mu}, \boldsymbol{\Sigma}) d\mathbf{x}}{\iint_{\text{CRF}} G(\mathbf{x}, \boldsymbol{\mu}, \boldsymbol{\Sigma}) d\mathbf{x}},$$

$$G(\mathbf{x}, \boldsymbol{\mu}, \boldsymbol{\Sigma}) = \frac{1}{\sqrt{|\boldsymbol{\Sigma}|} (2\pi)^2} \exp\left(-\frac{1}{2}(\mathbf{x} - \boldsymbol{\mu}) \boldsymbol{\Sigma}^{-1} (\mathbf{x} - \boldsymbol{\mu})^T\right),$$

$$\mathbf{x} = (x, y), \quad \boldsymbol{\mu} = (\mu_x, \mu_y), \quad \boldsymbol{\Sigma} = \begin{bmatrix} \sigma^2 & 0 \\ 0 & \sigma^2 \end{bmatrix},$$

where 'CRF' is a region of CRF; 'CRF  $\cap$  STM<sub>cent</sub>' is a region common to a CRF and a center stimulus in the cortical field (x,y);  $(\mu_x, \mu_y)$  is the mean position of the CRF center;  $\sigma$  is the standard deviation of the CRF center displacement; and  $G$  is the two-dimensional normal distribution that we hypothesized.

To quantify the strength of orientation selectivity, we used the following orientation selectivity index (OSI):

$$\text{OSI} = (a^2 + b^2)^{1/2} / \sum_{m=-5}^6 R_{\text{cent}}^{\text{conn}}(\theta_m),$$

where

$$a = \sum_{m^{\text{conn}}=-5}^6 R_{\text{cent}}^{\text{conn}}(\theta_m) \cos(2\theta_m), \text{ and } b = \sum_{m^{\text{conn}}=-5}^6 R_{\text{cent}}^{\text{conn}}(\theta_m) \sin(2\theta_m).$$

The OSI is a continuous metric with values ranging from 0 (non-selective) to 1 (perfectly selective). To quantify the degree of contextual modulation, we introduced the contextual modulation index (CMI) defined as follows:

$$\text{CMI} = (\Delta R_{\text{iso-orientation}}^{\text{conn}} - \Delta R_{\text{cross-orientation}}^{\text{conn}}) / (\Delta R_{\text{iso-orientation}}^{\text{conn}} + \Delta R_{\text{cross-orientation}}^{\text{conn}}),$$

$$\Delta R_{\text{iso-orientation}}^{\text{conn}} = R_{\text{cent}}^{\text{conn}}(0) - R_{\text{cent+surr}}^{\text{conn}}(0,0),$$

$$\Delta R_{\text{cross-orientation}}^{\text{conn}} = R_{\text{cent}}^{\text{conn}}(0) - R_{\text{cent+surr}}^{\text{conn}}(0,90).$$

A negative CMI indicates that suppression by cross-orientation surrounding stimuli is stronger than by iso-orientation surrounding stimuli; a positive CMI indicates the opposite. In particular, a CMI greater than 1 indicates that the response is enhanced by iso-orientation stimuli in the surround. Furthermore, the strength of iso-orientation suppression was defined as  $1 - R_{\text{cent+surr}}^{\text{conn}}(0,0)/R_{\text{cent}}^{\text{conn}}(0)$ ; the strength of cross-orientation facilitation was defined as  $R_{\text{cent+surr}}^{\text{conn}}(0,90)/R_{\text{cent}}^{\text{conn}}(0) - 1$ .

- Hubel, D. H. & Wiesel, T. N. Receptive fields and functional architecture of monkey striate cortex. *J. Physiol. (Lond.)* **195**, 215–243 (1968).
- Hubel, D. H. & Wiesel, T. N. Receptive fields, binocular interaction and functional architecture in the cat's visual cortex. *J. Physiol. (Lond.)* **160**, 106–154 (1962).
- Zipser, K., Lamme, V. A. F. & Schiller, P. H. Contextual modulation in primary visual cortex. *J. Neurosci.* **16**, 7376–7389 (1996).
- Akasaki, T., Sato, H., Yoshimura, Y., Ozeki, H. & Shimegi, S. Suppressing effects of receptive field surround on neuronal activity in the cat primary visual cortex. *Neurosci. Res.* **43**, 207–220 (2002).
- Jones, H. E., Wang, W. & Litalo, A. M. Spatial organization and magnitude of orientation contrast interactions in primate V1. *J. Neurophysiol.* **88**, 2796–2808 (2002).
- Sengpiel, F., Sen, A. & Blakemore, C. Characteristics of surround inhibition in cat area 17. *Exp. Brain Res.* **116**, 216–228 (1997).
- Knierim, J. J. & Van Essen, D. C. Neuronal responses to static texture patterns in area V1 of the alert macaque monkey. *J. Neurophysiol.* **67**, 961–980 (1992).
- Nothdurft, H. C., Gallant, J. L. & Van Essen, D. C. Response modulation by texture surround in primate area V1: correlates of "popout" under anesthesia. *Vis. Neurosci.* **16**, 15–34 (1999).
- Das, A. & Gilbert, C. D. Topography of contextual modulations mediated by short-range interactions in primary visual cortex. *Nature* **399**, 655–661 (1999).
- Hubel, D. H. & Wiesel, T. N. Shape and arrangement of columns in cat's striate cortex. *J. Physiol. (Lond.)* **165**, 559–568 (1963).
- Hubel, D. H. & Wiesel, T. N. Sequence regularity and geometry of orientation columns in the monkey striate cortex. *J. Comp. Neurol.* **158**, 267–293 (1974).
- Blasdel, G. G. & Salama, G. Voltage-sensitive dyes reveal a modular organization in monkey striate cortex. *Nature* **321**, 579–585 (1986).
- Bonhoeffer, T. & Grinvald, A. Iso-orientation domains in cat visual cortex are arranged in pinwheel-like patterns. *Nature* **353**, 429–431 (1991).
- Malach, R., Amir, Y., Harel, M. & Grinvald, A. Relationship between intrinsic connections and functional architecture revealed by optical imaging and in vivo targeted biocytin injections in primate striate cortex. *Proc. Natl. Acad. Sci. U. S. A.* **90**, 10469–10473 (1993).



15. Stettler, D. D., Das, A., Bennett, J. & Gilbert, C. D. Lateral connectivity and contextual interactions in macaque primary visual cortex. *Neuron* **36**, 739–750 (2002).
16. Ohki, K. *et al.* Highly ordered arrangement of single neurons in orientation pinwheels. *Nature* **442**, 925–928 (2006).
17. Smith, M. A. & Kohn, A. Spatial and temporal scales of neuronal correlation in primary visual cortex. *J. Neurosci.* **28**, 12591–12603 (2008).
18. Monier, C., Chavane, F., Baudot, P., Graham, L. J. & Frégnac, Y. Orientation and direction selectivity of synaptic inputs in visual cortical neurons: a diversity of combinations produces spike tuning. *Neuron* **37**, 663–680 (2003).
19. Tanifuji, M., Sugiyama, T. & Murase, K. Horizontal propagation of excitation in rat visual cortical slices revealed by optical imaging. *Science* **266**, 1057–1059 (1994).
20. Connor, C. E., Brincat, S. L. & Pasupathy, A. Transformation of shape information in the ventral pathway. *Curr. Opin. Neurobiol.* **17**, 140–147 (2007).
21. Dalva, M. B. Remodeling of inhibitory synaptic connections in developing ferret visual cortex. *Neural Dev* **5**, 5 (2010).
22. Nauhaus, I., Benucci, A., Carandini, M. & Ringach, D. L. Neuronal selectivity and local map structure in visual cortex. *Neuron* **57**, 673–679 (2008).
23. Maldonado, P. E., Gödecke, I., Gray, C. M. & Bonhoeffer, T. Orientation selectivity in pinwheel centers in cat striate cortex. *Science* **276**, 1551–1555 (1997).
24. Bair, W., Cavanaugh, J. R. & Movshon, J. A. Time course and time-distance relationships for surround suppression in macaque V1 neurons. *J. Neurosci.* **23**, 7690–7701 (2003).
25. Hubel, D. H. & Wiesel, T. N. Uniformity of monkey striate cortex: a parallel relationship between field size, scatter, and magnification factor. *J. Comp. Neurol.* **158**, 295–305 (1974).
26. Dow, B. M., Snyder, A. Z., Vautin, R. G. & Bauer, R. Magnification factor and receptive field size in foveal striate cortex of the monkey. *Exp. Brain Res.* **44**, 213–228 (1981).
27. Van Essen, D. C., Newsome, W. T. & Maunsell, J. H. R. The visual field representation in striate cortex of the macaque monkey: asymmetries, anisotropies, and individual variability. *Vision Res.* **24**, 429–448 (1984).
28. Alexander, D. M. & Van Leeuwen, C. Mapping of contextual modulation in the population response of primary visual cortex. *Cogn. Neurodyn.* **4**, 1–24 (2009).
29. Yao, H. & Li, C. Y. Clustered organization of neurons with similar extra-receptive field properties in the primary visual cortex. *Neuron* **35**, 547–553 (2002).
30. Blasdel, G. G. Orientation selectivity, preference, and continuity in monkey striate cortex. *J. Neurosci.* **12**, 3139–3161 (1992).
31. Schwabe, L., Obermayer, K., Angelucci, A. & Bressloff, P. C. The role of feedback in shaping the extra-classical receptive field of cortical neurons: a recurrent network model. *J. Neurosci.* **26**, 9117–9129 (2006).
32. Carandini, M., Movshon, J. A. & Ferster, D. Pattern adaptation and cross-orientation interactions in the primary visual cortex. *Neuropharmacology* **37**, 501–511 (1998).
33. Mariño, J. *et al.* Invariant computations in local cortical networks with balanced excitation and inhibition. *Nat. Neurosci.* **8**, 194–201 (2005).
34. Schummers, J., Mariño, J. & Sur, M. Local networks in visual cortex and their influence on neuronal responses and dynamics. *J. Physiol. Paris* **98**, 429–441 (2004).
35. Schummers, J., Mariño, J. & Sur, M. Synaptic integration by V1 neurons depends on location within the orientation map. *Neuron* **36**, 969–978 (2002).
36. Ferster, D., Chung, S. & Wheat, H. Orientation selectivity of thalamic input to simple cells of cat visual cortex. *Nature* **380**, 249–252 (1996).
37. Chapman, B., Zahs, K. R. & Stryker, M. P. Relation of cortical cell orientation selectivity to alignment of receptive fields of the geniculocortical afferents that arborize within a single orientation column in ferret visual cortex. *J. Neurosci.* **11**, 1347–1358 (1991).
38. Dragoi, V., Rivadulla, C. & Sur, M. Foci of orientation plasticity in visual cortex. *Nature* **411**, 80–86 (2001).
39. Roberts, M., Delicato, L. S., Herrero, J., Gieselmann, M. A. & Thiele, A. Attention alters spatial integration in macaque V1 in an eccentricity-dependent manner. *Nat. Neurosci.* **10**, 1483–1491 (2007).
40. Wielaard, J. & Sajda, P. Extraclassical receptive field phenomena and short-range connectivity in V1. *Cereb. Cortex* **16**, 1531–1545 (2006).
41. Okamoto, T., Watanabe, M., Aihara, K. & Kondo, S. An explanation of contextual modulation by short-range isotropic connections and orientation map geometry in the primary visual cortex. *Biol. Cybern.* **91**, 396–407 (2004).
42. Schwartz, O., Hsu, A. & Dayan, P. Space and time in visual context. *Nat Rev Neurosci* **8**, 522–535 (2007).
43. Kisvárdy, Z. F., Tóth, É., Rausch, M. & Eysel, U. T. Orientation-specific relationship between populations of excitatory and inhibitory lateral connections in the visual cortex of the cat. *Cereb. Cortex* **7**, 605–618 (1997).
44. Gilbert, C. D. & Wiesel, T. N. Clustered intrinsic connections in cat visual cortex. *J. Neurosci.* **3**, 1116–1133 (1983).
45. Somers, D. C. *et al.* A local circuit approach to understanding integration of long-range inputs in primary visual cortex. *Cereb. Cortex* **8**, 204–217 (1998).
46. Ozeki, H. *et al.* Relationship between excitation and inhibition underlying size tuning and contextual response modulation in the cat primary visual cortex. *J. Neurosci.* **24**, 1428–1438 (2004).
47. Tamura, H., Kaneko, H., Kawasaki, K. & Fujita, I. Presumed inhibitory neurons in the macaque inferior temporal cortex: visual response properties and functional interactions with adjacent neurons. *J. Neurophysiol.* **91**, 2782–2796 (2004).
48. Grinvald, A. *et al.* in *Modern Techniques in Neuroscience Research* (eds. Windhorst, U. & Johansson, H.) 893–969 (Springer-Verlag, 1999).
49. Yokoo, T., Knight, B. W. & Sirovich, L. An optimization approach to signal extraction from noisy multivariate data. *Neuroimage* **14**, 1309–1326 (2001).
50. Serié, P., Latham, P. E. & Pouget, A. Tuning curve sharpening for orientation selectivity: coding efficiency and the impact of correlations. *Nat. Neurosci.* **7**, 1129–1135 (2004).
51. Ernst, U. A., Pawelzik, K. R., Sahar-Pikielny, C. & Tsodyks, M. V. Intracortical origin of visual maps. *Nat. Neurosci.* **4**, 431–436 (2001).
52. Kang, K., Shelley, M. & Sompolinsky, H. Mexican hats and pinwheels in visual cortex. *Proc. Natl. Acad. Sci. U. S. A.* **100**, 2848–2853 (2003).
53. Carreira-Perpiñán, M. Á. & Goodhill, G. J. Influence of lateral connections on the structure of cortical maps. *J. Neurophysiol.* **92**, 2947–2959 (2004).

## Acknowledgements

The work was supported by the Aihara Complexity Modelling Project, an ERATO grant from the Japan Science and Technology Agency (K.A.), a CREST grant from the Japan Science and Technology Agency (I.F.), and the Funding Program for World-Leading Innovative R&D on Science and Technology (FIRST Program) from the Japan Society for the Promotion of Science, initiated by the Council for Science and Technology Policy (CSTP) (K.A.).

## Author contributions

T.O. designed the study, analyzed the data, and carried out the simulation together with M.W. and K.A. K.I., H.T. and I.F. carried out the optical imaging experiment. T.O., K.I., H.T. and I.F. co-wrote the manuscript. All the authors commented on the manuscript.

## Additional information

**Supplementary information** accompanies this paper at <http://www.nature.com/scientificreports>

**Competing financial interests:** The authors declare that they have no competing financial interests relevant to this work.

**License:** This work is licensed under a Creative Commons Attribution-NonCommercial-ShareAlike 3.0 Unported License. To view a copy of this license, visit <http://creativecommons.org/licenses/by-nc-sa/3.0/>

**How to cite this article:** Okamoto, T. *et al.* Predicted contextual modulation varies with distance from pinwheel centers in the orientation preference map. *Sci. Rep.* **1**, 114; DOI:10.1038/srep00114 (2011).